2023 IEEE International Conference on Robotics and Automation (ICRA 2023)
May 29 - June 2, 2023. London, UK

Task-Oriented Stiffness Setting for a Variable Stiffness Hand

Ana Elvira H. Martin[1], Ashok M. Sundaram[1], Werner Friedl[1], Virginia Ruiz Garate[2] and Máximo A. Roa[1]

***Abstract*— The integration of variable stiffness actuators (VSA) in robotic systems endows them with intrinsic flexibility and therefore robustness to unknown disturbances. However, this characteristic presents a challenge: choosing the best intrinsic stiffness setting guaranteeing the required force application capability while keeping the system as adaptable to uncertainties as possible. This paper proposes a method to set the optimal stiffness for a multi-finger VSA hand to perform a desired manipulation task. The task is generically represented as a force (with unknown magnitude) applied along a reference direction. According to the force application's direction and the hand's kinematic state, the fingers assume a certain role to split the collective force application. We employ the endpoint stiffness ellipsoid to analyze the required finger stiffness to fulfill the task. We evaluate the optimized stiffness settings in a door opening application with an iterative adaption of the stiffness behavior to handle the unknown force requirement. The results show a successful collective behavior of the fingers, where the stiffness setting considers a task-oriented force-adaptability trade-off and effective use of independent VSA fingers.**

I. Introduction

In the last decades, task-space impedance controllers have been proposed to provide an active compliant behavior in rigid robotic systems [1]. Typical applications involve safe interactions with lightweight arms [2], dexterous dual-arm manipulation, and multi-fingered grasping [3], [4]. Passive mechanical compliance can also be achieved using VSA in robotic systems, providing increased robustness and passive adaptability for interactions in unstructured environments. Typical examples of this technology are tendon-driven VSA hands, including the Awiwi hand [5], the Pisa/IIT Soft Hand [6], or the CLASH Hand [7]. The combination of passive mechanical and active compliance (provided by the controller) [8] can improve the system's robustness by further changing the perceived stiffness behavior (intrinsically) even when the control gains have reached the limit provided by the dynamics of the system and actuators' torque limits. However, an open challenge when dealing with intrinsic variable stiffness is setting the stiffness value required to execute a desired task. Current approaches to find a suitable stiffness setting can be broadly classified into:

a) Using pre-defined stiffness levels: involves setting a stiffness value that remains constant throughout the task, as shown in [9] (application of the controller [10]). Multiple discrete stiffness levels (low-, medium-, and high) are used in [11] through a decision tree to determine the stiffness level for a grasping task. These practical solutions do not exploit the whole stiffness variation range.

b) Transference of human stiffness data: Human stiffness data are gathered (e.g., using EMG sensors) and then transferred directly to the robot [12], [13]. Typical applications are teleoperation of manipulators for online collaboration [14], prosthetic devices [15], or learning from demonstration [16]. This approach requires dealing with complex data acquisition and having a suitable method to process and map the sensor data to an actual stiffness value. Typically it uses coordinated stiffness variation patterns for the complete system, to lower the complexity of the robot control system. However, it limits the independent variation of stiffness in the joints, which limits the variety of stiffness behaviors available, thus in the case of multiple fingers, it limits their collaboration.

c) Using stiffness matrices and ellipsoids: The current or desired stiffness capabilities of the system can be graphically represented as stiffness ellipsoids. This representation can be combined with an optimization approach to approximate the desired stiffness through a suitable joint stiffness and configuration setting, as explained in Section II. The numerical optimization of the 6×6 grasp- [17] or endpoint- [18] stiffness matrices, require setting target values for all the elements in the matrices, which are both complex to obtain

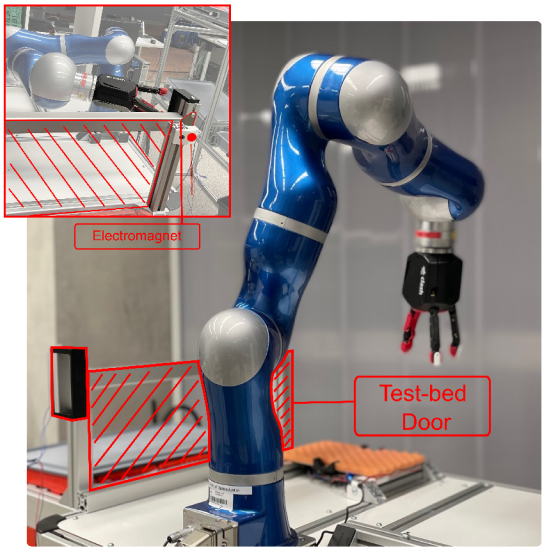

Fig. 1. Experimental setup showing the DLR CLASH hand pulling the door handle (in red) of our testbed door frame. The electromagnet in the back side of the handle allows us to simulate different holding forces, that remain unknown to the system during our experiments.

This work has received funding from the European Union's Horizon Europe research and innovation program under grant agreement No.101070600, project SoftEnable. [1] All the authors are with the Institute of Robotics and Mechatronics, German Aerospace Center (DLR), 82234 Wessling, Germany. [2] V. Ruiz is with Mondragon Unibertsitatea, Faculty of Engineering, Bilbao, Spain; with University of the West of England, Bristol, United Kingdom; and Bristol Robotics Laboratory. Contact: ana.huezomartin@dlr.de

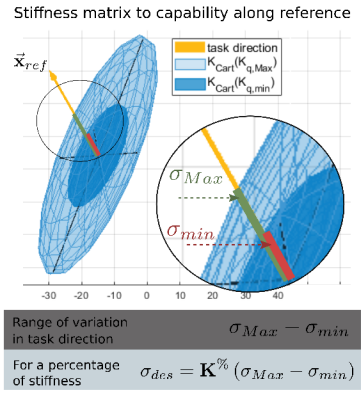

Fig. 2. The range of variation of stiffness variation for the direction of interest is is computed as σ_{Max}-σ_{min}. The desired stiffness behavior σ_{des} is obtained as a percentage $K^{\%}$ of the range of variation of stiffness

and counter-intuitive for the user to set.

As an alternative, the 3D stiffness ellipsoid is easier to associate with a task-space behavior, thus more intuitive for the user to set a target behavior. In [19], [20], the grasp stiffness ellipsoid's orientation and shape are optimized, reducing the precision but ensuring the minimal required grasp stiffness behavior. On the same line, the configuration of a redundant manipulator is optimized in [21] by targeting the maximum *task compatibility index* proposed in [22], which provides the maximum elongation of the force and stiffness ellipsoid in the task direction. This allows setting a target behavior by only giving a reference direction for the optimization. Furthermore, the stiffness setting can change for different manipulation phases, e.g., an *approach phase*, where the arm/hand is positioned with respect to the intended object, a *closing/grasping* phase where the hand is closed around the object, and a *core- manipulation phase* where forces are applied on the object along a specific direction to perform the desired manipulation action.
The purpose of our work is subdivided in the following objectives: A) task compatible optimization of a stiffness setting, during the *core-manipulation phase*, defined by the desired direction of force application $\vec{\mathbf{x}}_{ref}$; B) exploitation of collaborative stiffness roles for our experimental multi-fingered VSA hand (CLASH [23]); C) boundary analysis of *endpoint stiffness capabilities*, an application of the compatibility index by [22] at the boundaries of the range of stiffness variation ($\sigma_{Max}, \sigma_{min}$), as shown in Fig. 2; and optimization of adaptive *target values* inside the boundary analysis, instead of targeting directly a maximum or minimum value. These lead to D) the optimal force-adaptability trade-off (see Fig. 3a) without knowledge of the required force by steadily increasing the *target values*.

All of these objetives will be carried out under the assumptions that: 1) the task can be described by translational force application, 2) only the intrinsic joint stiffness variation contributes to the stiffness behavior, and 3) a complete knowledge of the system's range of stiffness variation is available.

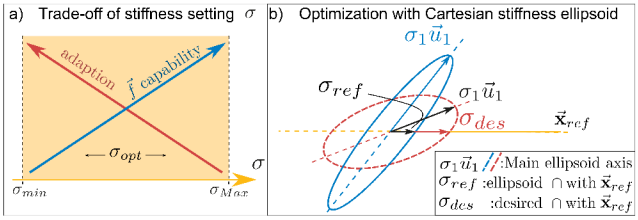

Fig. 3. a) The optimal stiffness value simultaneously provides the highest compliance and the task's minimum required force application. b) Optimization process. The desired task direction $\vec{\mathbf{x}}_{ref}$ in yellow, and the initial and optimized endpoint stiffness ellipsoids in blue and red, resp. with the stiffness capabilities σ_{ref} and σ_{des} along $\vec{\mathbf{x}}_{ref}$.

II. Methodology

This section presents the method for obtaining an optimal stiffness setting in order to provide a task-oriented collaboration of the fingers in a multi-finger hand. It starts with a brief mathematical background. Afterward, we describe in detail the core-manipulation task, subdivided into the manipulation and internal stiffness parts, and the proposed approach to obtain a coordinated collaboration of the fingers for task completion using adaptable stiffness.

A. Mathematical Background

The grasp stiffness matrix $\mathbf{K} \in \mathbb{R}^{6\times6}$ is a symmetric matrix that provides a relation between the wrench $\Delta\mathbf{w} \in \mathbb{R}^6$ applied to an object and the object's displacement $\Delta\mathbf{u} \in \mathbb{R}^6$,

$$\Delta\mathbf{w} = \mathbf{K}\Delta\mathbf{u} = \left(\mathbf{G}\mathbf{K}_c\mathbf{G}^T\right)\Delta\mathbf{u}, \tag{1}$$

where $\mathbf{G} \in \mathbb{R}^{6\times3n_c}$ is the grasp matrix for n_c Hard Finger contacts [20], which relates the contact forces and moments transmitted through the contact points to a net wrench on the object. The contact stiffness matrix $\mathbf{K}_c \in \mathbb{R}^{3n_c\times3n_c}$ contains the Cartesian stiffness matrices at each contact point.
We focus our analysis on the stiffness behavior produced by the passive joint stiffness variation. Consequently,

$$\mathbf{K}_c = \left(\mathbf{J}_{hand}\mathbf{K}_q^{-1}\mathbf{J}_{hand}^T\right)^{-1}, \tag{2}$$

where $\mathbf{J}_{hand} \in \mathbb{R}^{3n_c\times n_h}$ is the hand Jacobian, $\mathbf{K}_q \in \mathbb{R}^{n_h\times n_h}$ the joint stiffness matrix, and n_h is the total number of joints in the N-fingered hand.

To visualize the stiffness behavior described by the numerical elements of a stiffness matrix, the translational or rotational stiffness can be represented as a 3D ellipsoid. From now on, we use the translational stiffness matrix, under the assumption that our task can be described by translational force requirements. For example, in the case of opening doors, we focus on pulling the doors open, and not in turning the handle of a door to open it.

As a future step, the extension of the methodology will also involve tasks with rotational force requirements.

Stiffness capability as a transmission ratio along a reference vector. We assume that the task requires a certain force application (and therefore a certain stiffness behavior) in a given direction $\vec{\mathbf{x}}_{ref,i} = [\vec{x}_{i,1}\vec{x}_{i,2}\vec{x}_{i,3}]^T$. We take advantage of the ellipsoidal representation of the stiffness capabilities by using the concept of *task compatibility index* [22], [21],

and we calculate the stiffness *transmission ratio* represented by the translational Cartesian stiffness matrix in the task direction with:

$$\left(\sigma_{ref}\frac{\vec{\mathbf{x}}_{ref}}{\|\vec{\mathbf{x}}_{ref}\|}\right)^{T}\mathbf{K}_{Cart}\left(\mathbf{J}(\mathbf{q})\mathbf{J}(\mathbf{q})^{T}\right)\mathbf{K}_{Cart}\left(\sigma_{ref}\frac{\vec{\mathbf{x}}_{ref}}{\|\vec{\mathbf{x}}_{ref}\|}\right)=1$$
$$\sigma_{ref}=\left(\frac{\vec{\mathbf{x}}_{ref}}{\|\vec{\mathbf{x}}_{ref}\|}^{T}\mathbf{K}_{Cart}\left(\mathbf{J}(\mathbf{q})\mathbf{J}(\mathbf{q})^{T}\right)\mathbf{K}_{Cart}\frac{\vec{\mathbf{x}}_{ref}}{\|\vec{\mathbf{x}}_{ref}\|}\right)^{-\frac{1}{2}} \quad (3)$$

such that the *transmission ratio* σ_{ref} corresponds geometrically to the length of the vector from the origin to the surface of the ellipsoid along the vector $\frac{\vec{\mathbf{x}}_{ref}}{\|\vec{\mathbf{x}}_{ref}\|}$. Thus σ_{ref} represents the actual stiffness or force application capabilities given by $\mathbf{K}_{Cart}$ along the normalized task direction $\frac{\vec{\mathbf{x}}_{ref}}{\|\vec{\mathbf{x}}_{ref}\|}$.

In contrast to previous joint stiffness optimization methods [18], [20], [19], [17] we use the stiffness transmission ratio or capability directly in our objective function. This allows prioritizing the approximation of the force application capabilities to a desired value, rather than the orientation of the ellipsoid in the task direction. Then, as discussed in [22], by calculating the stiffness capabilities in the direction of interest we compute the effect (or transmission ratio) of the ellipsoid's shape, volume and orientation in the task direction. This ensures the optimization of all the ellipsoid's characteristics at once for the given interest direction.

To approximate the desired force application capabilities we build the cost function:

$$\min_{\mathbf{K}_q}\quad \mathbf{V}_i=\sum^{i}\|\left(\sigma_{ref,i}-\sigma_{des,i}\right)\|\,\mathbf{V}_i\left(\sigma_{ref,i}\right) \quad (4)$$

such that the sub-index $i\in\mathbb{N}[1,N]$ (for N-fingered hand) allows a cost function for each finger, in a case where the fingers have either different reference directions $\vec{\mathbf{x}}_{ref,i}$ or different desired behaviors $\sigma_{des,i}$. The proposed optimization *wrt* the joint stiffness matrix $\mathbf{K}_q$, will find the optimal intrinsic joint stiffness values to achieve the target stiffness behavior.

By minimizing the error between the stiffness capability σ_{ref} and the σ_{des} we seek to approximate a stiffness behavior at any point inside the range of stiffness variation $(\sigma_{Max}-\sigma_{min})$. Setting the desired behavior σ_{des} equal to σ_{Max} would directly produce the maximization of stiffness along a desired direction, as proposed by [21]. However, we want to set the minimum stiffness, within the allowed stiffness range, that fulfills the task (see Fig. 3a). *The range of endpoint stiffness variation in the task direction* is calculated as shown in Fig. 2, computing the endpoint stiffness matrix for each virtual contact point:

$$\mathbf{K}_{Cart}=\left(\mathbf{J}(\mathbf{q})\mathbf{K}_q^{-1}\mathbf{J}(\mathbf{q})^{T}\right)^{-1} \quad (5)$$

and switching between maximum and minimum joint stiffness matrices $\mathbf{K}_q$ (which are values given by the hardware capabilities). Eq. 3 provides then the corresponding stiffness capabilities boundaries in the reference direction $\vec{\mathbf{x}}_{ref}$.

We set the target stiffness behavior as a percentage of stiffness inside the computed variation range. In addition, we propose to set the desired behavior by iteratively increasing

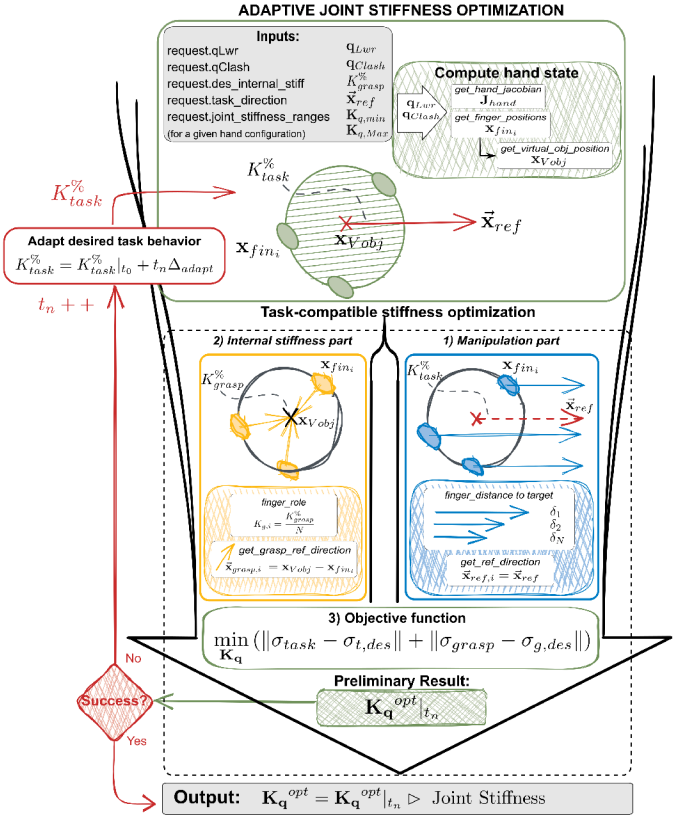

Fig. 4. Adaptive optimization pipeline to set the task-oriented stiffness, with two main parts: analysis of the manipulation (blue) and analysis of internal stiffness (yellow). On the left side, in red, the desired task behavior is updated and increased by Δ_{adapt} with every unsuccessful execution.

the stiffness value, starting at the lower boundary of stiffness variation. This can easily be adapted to a preferred setting by the user. This ensures the maximum adaptability when the task is successfully executed (therefore meeting the minimum force requirement), as illustrated by the force-adaptability trade-off in Fig. 3a.

B. Task-compatible stiffness optimization

The proposed optimization approach is depicted in Fig. 4. We assume the system receives as input from the user or a high-level planner the direction of the manipulation task ($\vec{\mathbf{x}}_{ref}$), the *desired internal stiffness* ($K^{\%}_{grasp}$, which regulates the stiffness of the current grasp), a *desired task behavior* ($K^{\%}_{task}$, which is adapted in order to fulfill the task requirements), and considers the hand state (which might influence the range of achievable stiffness). The analysis of the core-manipulation phase is divided into a manipulation and an internal stiffness part, each part with its own requirements in terms of stiffness. In the *manipulation part*, the target force application behavior is splitted among the fingers according to their potential *role* in the manipulation task (which depends on the location of the fingers with respect to the task direction), thus resulting in a *stiffness behavior* for each finger in the task direction. The *internal stiffness part* keeps a hold on the object (after the *closing/grasping* phase), but adapts the stiffness to increase the hold on the object during the manipulation execution. Therefore, the internal

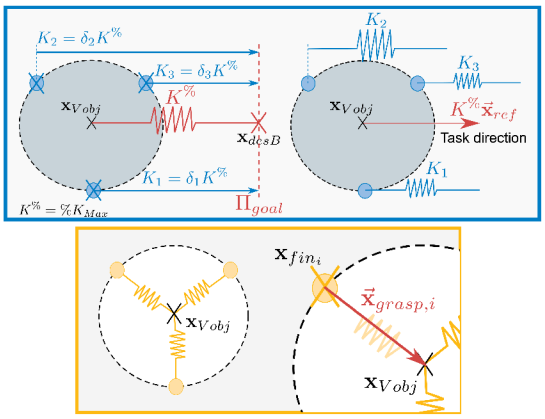

Fig. 5. Top: Division of the desired stiffness behavior among the fingertips, in order to assign a finger stiffness role (stiffness direction and magnitude). Bottom: Virtual model for a three-finger grasp, shows the virtual internal contact forces that will be regulated with the desired internal stiffness. The reference direction is estimated and associated with each finger.

stiffness is equally divided among all fingers[1] and, using a virtual object frame as in [24] a stiffness in direction of the virtual contact forces is defined for each finger. We assume that there is just one contact point per fingertip, $n_c \equiv N$. We assume as well that the joint configuration during the task execution is constant and not affected by the setting of the stiffness (which is feasible in the CLASH hand). The two parts of the analysis are explained in detail below.

1) Manipulation part: We analyze the contributions that each finger should provide to the collective goal for dividing the stiffness behavior among the fingers and assign, accordingly, an active or passive involvement in the manipulation task (as sketched with arrows in the blue section of Fig. 4).

On the left side of Fig. 5 (top), we show how the desired stiffness behavior $K^{\%}_{task}$ (depicted as a red spring) is divided and assigned to each fingertip. We use the relative position of each fingertip *wrt* to the collective goal to define the magnitude K_i that each fingertip i will contribute to the collective desired behavior. Using the point to plane distance, and therefore considering the collective goal as *goal plane* Π_{goal}, the magnitude of each K_i holds the following relation to the distance values δ_i:

$$\begin{aligned} \delta_i &= \left\langle \left(\mathbf{x}^W_{fin_i} - \mathbf{x}^W_{desB}\right), \vec{\mathbf{x}}_{ref} \right\rangle \\ \frac{K_i}{\delta_i} &= \frac{K_{i+1}}{\delta_{i+1}} = \ldots = \frac{K_N}{\delta_N} \end{aligned} \tag{6}$$

where $\mathbf{x}^W_{desB}$ is a goal coordinate computed from the center point of the fingers $\mathbf{x}_{Vobj}$ with addition of the desired behavior, $\mathbf{x}^W_{desB} = \mathbf{x}_{Vobj} + 1\vec{\mathbf{x}}_{ref}, \forall \delta_i \neq 0$ [2]. The reference vector $\vec{\mathbf{x}}_{ref}$ is used as a normal vector to describe the collective *goal plane* (marked by a dotted line in Fig. 5 (top)), and $\langle , \rangle$ indicates the dot product of two vectors. Each value of desired contact stiffness K_i of the fingers will contribute to create the resulting collective behavior according to:

[1]Adjust for different stiffness capabilities using as weight the ratio between the smallest and greatest stiffness capability.

[2]According to the proposed relation between the δ_i and task involvement of finger-i, $\delta_i = 0$ implies $K_i \to 0$.

$$\frac{1}{K^{\%}_{task}} = \sum_{i=1}^{N} \frac{1}{K_i}. \tag{7}$$

Each K_i can be expressed in terms of a single independent unknown variable, e.g. K_1, so that Eq. 7 leads to the value of that unknown variable.

The final division of behaviors is depicted on the right side in Fig. 5 (top). Finally, using Eq. 3 we obtain the corresponding target stiffness capabilities $\sigma_{t,des_i} = \sigma(K_i)$ corresponding to each desired stiffness behavior K_i of the fingers.

2) Internal stiffness part: In order to adjust the compliant behavior inside the hand, we make use of the virtual object frame model presented in [3]. For this, we connect the fingertips to a virtual object frame, defined by:

$$\mathbf{x}^W_{Vobj} = \frac{\sum_1^N \mathbf{x}^W_{fin_i}}{N} \tag{8}$$

where $\mathbf{x}^W_{Vobj}$ is the position of the virtual object frame, $\mathbf{x}^W_{fin_i}$ represent the position vectors of each of the finger virtual contacts *wrt* world coordinate frame, and N indicates the total number of fingers. In the case of the CLASH hand, for instance, the spring-like behavior towards $\mathbf{x}^W_{Vobj}$ is provided by the actual intrinsic compliance of CLASH.

Using the vector connecting each contact point to the virtual object frame we compute a reference direction $\vec{\mathbf{x}}_{grasp,i}$ for the optimization of each contact point stiffness ellipsoid (see Fig. 5 (bottom)). This reference direction represents the virtual contact forces that characterize our grasp virtual model, defined as follows:

$$\vec{\mathbf{x}}_{grasp,i} = \mathbf{x}^W_{Vobj} - \mathbf{x}^W_{fin_i} \tag{9}$$

where $\vec{\mathbf{x}}_{grasp,i}$ is the reference direction of internal stiffness of the finger i. The magnitude of the desired stiffness behavior for this part is equal in all fingers seeking to maintain a balance of the contact forces, and the value is defined by the desired grasp stiffness $K^{\%}_{grasp}$ such that $K_{g,i} = \frac{K^{\%}_{grasp}}{N}$. Finally, the corresponding target internal stiffness σ_{g,des_i} is computed by using Eq. 3, as shown in Fig. 2.

3) Objective function: As a last step, we introduce the stiffness goals in Eq. 4 and obtain:

$$\min_{\mathbf{K_q}} \left(\|\sigma_{grasp,i} - \sigma_{g,des_i}\| + \|\sigma_{task,i} - \sigma_{t,des_i}\| \right) \tag{10}$$

such that σ_{t,des_i} and σ_{g,des_i} are the finger target stiffness behaviors for the manipulation and internal stiffness parts of the core-manipulation task, that have been computed along this subsection. $\sigma_{task,i}$ and $\sigma_{grasp,i}$ are the current stiffness capabilities of the fingers (for the manipulation and internal stiffness part respectively), which should be approximated to the desired behaviors.

III. Implementation

For verifying the proposed approach, we use the DLR CLASH hand [23] mounted on a DLR Light-Weight Robot arm (LWR) (see Fig. 1). The CLASH hand uses tendon-based variable joint compliance and provides interfaces to control the passive finger stiffness and joint positions independently.

a) Optimization: To ensure that the optimal joint stiffness values are achievable in our system, we compute the set of feasible joint stiffness matrices $\mathbf{K}_{q,i}$ and save them in a Look-up Table [7]. The proposed approach will find the joint stiffness matrices that produce the closest stiffness behavior in the reference direction $\vec{\mathbf{x}}_{ref}$.

b) Dealing with joint stiffness coupling between fingers: In CLASH we are able to regulate the stiffness of the thumb separately from the stiffness of the index fingers. However, as shown in Eq. 7 the K_i stiffness for both index fingers depends on the same joint stiffness matrix.

For dealing with the collective behavior, calculated in Section II-B.1, in the case of coupled fingers, we compute an average distance value δ_{index} and consequently an average finger stiffness role for the coupled fingers, as follows: $\delta_{index} = \frac{2\delta_i\delta_j}{\delta_i+\delta_j}$, such that δ_i, δ_j represent the finger stiffness role of corresponding left- and right index finger.

IV. Experimental Evaluation

To test the proposed approach, we use as testbed a door frame (marked in red in Fig. 1) with different holding forces (the *unknown required force*). The evaluation is similar to the task of opening a fridge door when the opening force is unknown. The task is described by giving a direction axis along which a force needs to be applied in order to successfully open the door.

For the evaluation of the approach, we choose a specific grasp of the handle, illustrated in Fig. 6. Note that the thumb and the index fingers are located at opposite side of the highlighted handle, which provides them with clearly different roles during the execution of the pulling task. The finger inside the handle will be the main driver of the task execution.

A. The experiment

Our algorithm provides the passive stiffness setting that will increase the force application capability along the desired direction, until the task can be successfully executed. The success of the task is a boolean value, qualified by a human observer.

Our approach will be compared with the *stiffness decision tree* used in [11], which assigns a finger stiffness value among three different discrete levels, according to the task. Our case is dealing with a non-fragile object, with high certainty of the object's location in a non-cluttered environment, therefore a medium *stiffness setting* is assigned to all fingers (0.5 stiffness setting). We add adaptability to this approach by defining fixed step-wise increments of the *stiffness setting*.

For the experiment, the robot repeatedly tries to pull open the test-bed door while it is held by 4 different forces. For each trial we apply once the step-wise stiffness setting adaptation (baseline method) followed by the same trial (force setting) with our task-compatible stiffness adaptation method. The stiffness adaptation will continue until either the task is successfully executed or the hardware's highest *stiffness setting* is reached. Finally, we compare the resulting stiffness settings commanded by each method to successfully open the test-bed door. We exploit the fact that our manipulation object can not fall-out of the hand during the manipulation and set initially the parameter $K^{\%}_{grasp} = 0\%$ to isolate the resulting collaboration between the fingers, given the task information.

TABLE I
Task-oriented vs Constant Stiffness Adaptation.

Task-oriented stiffness adaptation

Trial	Door F	Success	$\sigma_{ref,stOpt}$ [-]	$\sigma_{ref,i}$ [-]	
1	9.3N	True	1.353	6.991	2.082
2	11N	True	1.498	10.36	2.174
3	13.4N	True	1.73	16.67	2.397
4	15.6N	False	1.978	25.15	2.667

Step-wise stiffness adaptation

Trial	Door F	Success	$\sigma_{ref,Const}$ [-]	$\sigma_{ref,i}$ [-]	
1	9.3N	True	1.662	18.71	2.265
2	11N	True	1.662	18.71	2.265
3	13.4N	True	1.763	20.23	2.397
4	15.6N	False	2.005	25.15	2.706

B. Experimental results and discussion

A summary of the experimental trials can be seen in Table I[3]. The upper half of Table I presents the stiffness behavior required to successfully execute the task, using our task-oriented stiffness optimization. The lower half provides the results of the step-wise increment of the stiffness setting.

Some characteristics in the optimization result are important goals in the test: an optimal trade-off between force application and adaptability, the compatibility with the task, collaborative behavior between the fingers, and the adaptation in cases that require application of higher forces.

The optimized force-adaptability trade-off can be observed clearly in Table I by comparing the stiffness capabilities used by each method to successfully open the door. The task-oriented adaptation manages to execute the task with lower stiffness than the baseline method, which reflects the exceeding stiffness (or lost adaptability) resulting from a step-wise adaptation of the *stiffness setting* instead of the *stiffness capability*. It is important to highlight that a reduced adaptability (by oversetting the stiffness values) makes the system more vulnerable to disturbances or hardware damage. To identify the task-compatibility of our results, we use a scenario where the task is executed along the same axis, but in opposite directions (e.g. pushing and pulling the handle). In this scenario we are able to observe in Fig. 6 (right side), through the endpoint stiffness ellipsoids, the opposite changes in the force application capabilities of the fingers. Using the middle stiffness setting as a base of comparison in blue, the red ellipsoids are larger or smaller according to the direction of the reference task vector, which shows task-compatible results. In the plots shown in Figs. 7-8 can be observed that in most of the trials the stiffness capability lies below the middle *stiffness setting* (yellow dotted line)

[3]Adaptation parameters in base-line method: Start *stiffness settings*$= 0.5$ with step-wise increase of 0.05. For the task-compatible optimization initial *desired behavior* $K^{\%}_{task}|_{t_0} = 0\%$ and $\Delta_{adapt} = 6\%$. In proximity to the upper stiffness boundary, the step-wise increase is: 0.01 and $\Delta_{adapt} = 1\%$.

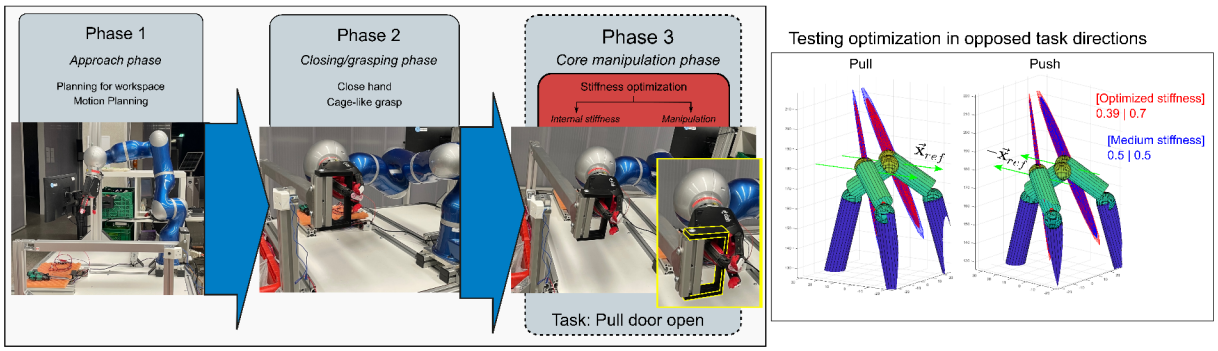

Fig. 6. Left: Complete task subdivided in three main phases: approach, closing/grasping, and (core) manipulation phase. Right: Resulting Cartesian stiffness ellipsoids at the virtual contact points, for opposite task directions ($\mathbf{x}_{ref}$). In blue, a constant stiffness setting for both actions; in red the optimized stiffness approach produces task-compatible capabilities for the index fingers.

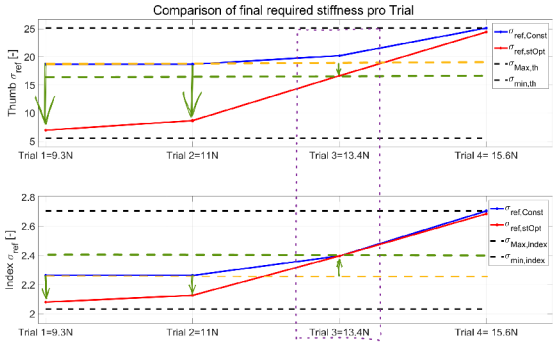

Fig. 7. Resulting finger stiffness behavior for successful task execution.

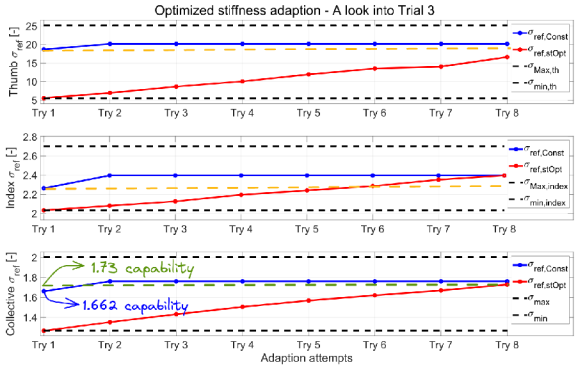

Fig. 8. A complete trial execution for both methods. The stiffness behavior is adapting in every attempt until the door is successfully opened. The plot shows the stiffness capabilities of the thumb (Top), one of the index fingers (Middle), and the collective stiffness behavior (Bottom).

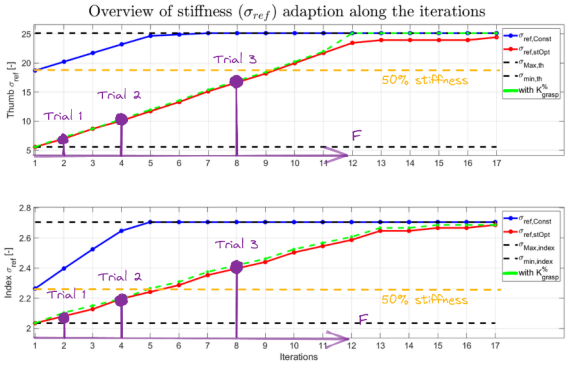

Fig. 9. Overall adaptation of the stiffness behavior for both methods. The marked *Trials* in purple indicate the number of attempts required to execute the task using our proposed adaptation. In green we show the added effect of the internal stiffness parameter $K^{\%}_{grasp}$.

defined as the starting point of adaptation in the baseline method. Therefore, the figure shows the adaptability lost when defining a fixed start setting of stiffness. In Fig. 7 we observe at *Trial 3* that each index requires the same capabilities in both methods to execute the task. In Fig. 8 we observe more closely the complete execution of *Trial 3* [4]. Note that the collective stiffness behavior increases, allowing the task execution even with the stiffness capabilities of the thumb below the middle level. The ability of adaptation and stiffness increase achieved by both methods can be observed in Fig. 9, as well as the small increase of the stiffness capabilities by using a $K^{\%}_{grasp} > 0$. The small difference made by this parameter is due to the constraint presented when targeting $K^{\%}_{task}$ too.

V. Conclusion

This work presented a planning method for setting joint stiffness values in multi-fingered soft hands with variable stiffness capabilities, through VSA. The joint stiffness values delivered by this approach allow to keep a higher adaptability while providing the minimum required force application capabilities for executing the task. The presented algorithm independently deals with each of the fingers, assigning them a different role according to their involvement in the manipulation task. The sub-division of the common behavior allows the fingers to take a passive or active role. Furthermore, it was observed that relying in the collective behavior of fingers with different stiffness roles contributes to more compliant results (more adaptability). The algorithm exploits the whole stiffness variation range available in the hand. The results are applicable for tasks defined by a force applied on a translational direction. As a next step, in an extension of this method, tasks involving rotational forces will be considered. Furthermore, a combination of passive and virtual stiffness and their effects to effectively exploit the stiffness capabilities of the system will also be explored.

[4]We do not compare the amount of 'Tries', to be able to open the door, but the resulting stiffness capabilities (the actual task requirements).

REFERENCES

[1] N. Hogan, "Impedance control - an approach to manipulation. i - theory. ii - implementation. iii - applications," *ASME J. of Dynamic Systems Measurement and Control*, vol. 107, pp. 1–24, 1985.

[2] A. De Luca, A. Albu-Schaffer, S. Haddadin, and G. Hirzinger, "Collision detection and safe reaction with the DLR-III lightweight manipulator arm," in *IEEE/RSJ Int. Conf. on Intelligent Robots and Systems*, 2006, pp. 1623–1630.

[3] T. Wimböck, C. Ott, and G. Hirzinger, "Passivity-based Object-Level Impedance Control for a Multfingered Hand," in *IEEE/RSJ Int. Conf. on Intelligent Robots and Systems*, 2006, pp. 4621–4627.

[4] T. Wimböck, C. Ott, A. Albu-Schäffer, and G. Hirzinger, "Comparison of object-level grasp controllers for dynamic dexterous manipulation," *Int. J. of Robotics Research*, vol. 31, no. 1, pp. 3–23, 2012.

[5] M. Grebenstein, M. Chalon, M. A. Roa, and C. Borst, "DLR multi-fingered hands," in *Humanoid Robotics: A Reference*, A. Goswami and P. Vadakkepat, Eds. Springer, 2019, pp. 481–522.

[6] M. G. Catalano, G. Grioli, E. Farnioli, A. Serio, M. Bonilla, M. Garabini, C. Piazza, M. Gabiccini, and A. Bicchi, "From Soft to Adaptive Synergies: The Pisa/IIT SoftHand," in *Human and Robot Hands: Sensorimotor Synergies to Bridge the Gap Between Neuroscience and Robotics*, M. Bianchi and A. Moscatelli, Eds. Springer, 2016, pp. 101–125.

[7] W. Friedl, H. Höppner, F. Schmidt, M. A. Roa, and M. Grebenstein, "CLASH: Compliant Low Cost Antagonistic Servo Hands," in *IEEE/RSJ Int. Conf. on Intelligent Robots and Systems*, 2018, pp. 6469–6476.

[8] M. Malvezzi and D. Prattichizzo, "Evaluation of grasp stiffness in underactuated compliant hands," in *IEEE Int. Conf. on Robotics and Automation*, 2013, pp. 2074–2079.

[9] M. Keppler and W. Sebastian. (2016) Robot david drilling and hammering into concrete. [Online]. Available: https://www.youtube.com/watch?v=JVdufPRK4NI

[10] M. Keppler, D. Lakatos, C. Ott, and A. Albu-Schäffer, "A passivity-based controller for motion tracking and damping assignment for compliantly actuated robots," in *IEEE Conf. on Decision and Control (CDC)*, 2016, pp. 1521–1528.

[11] A. M. Sundaram, W. Friedl, and M. A. Roa, "Environment-Aware Grasp Strategy Planning in Clutter for a Variable Stiffness Hand," in *IEEE/RSJ Int. Conf. on Intelligent Robots and Systems*, 2020, pp. 9377–9384.

[12] A. Ajoudani, N. G. Tsagarakis, and A. Bicchi, "Tele-impedance: Towards transferring human impedance regulation skills to robots," in *IEEE Int. Conf. on Robotics and Automation*, 2012, pp. 382–388.

[13] A. Ajoudani, *Transferring Human Impedance Regulation Skills to Robots*, ser. Springer Tracts in Advanced Robotics. Springer, 2016, vol. 110.

[14] L. Peternel, N. Tsagarakis, and A. Ajoudani, "Towards multi-modal intention interfaces for human-robot co-manipulation," in *IEEE/RSJ Int. Conf. on Intelligent Robots and Systems*, 2016, pp. 2663–2669.

[15] P. Capsi-Morales, C. Piazza, M. G. Catalano, A. Bicchi, and G. Grioli, "Exploring stiffness modulation in prosthetic hands and its perceived function in manipulation and social interaction," *Frontiers in Neurorobotics*, vol. 14, 2020.

[16] Y. Wu, F. Zhao, T. Tao, and A. Ajoudani, "A framework for autonomous impedance regulation of robots based on imitation learning and optimal control," *IEEE Robotics and Automation Letters*, vol. 6, no. 1, pp. 127–134, 2021.

[17] V. Ruiz Garate, N. Tsagarakis, A. Bicchi, and A. Ajoudani, "On the common-mode and configuration-dependent stiffness control of multiple degrees of freedom hands," in *IEEE-RAS Int. Conf. on Humanoid Robotics*, 2017, pp. 113–120.

[18] A. Albu-Schäffer, M. Fischer, G. Schreiber, F. Schoeppe, and G. Hirzinger, "Soft robotics: What Cartesian stiffness can obtain with passively compliant, uncoupled joints?" in *IEEE/RSJ Int. Conf. on Intelligent Robots and Systems*, vol. 4, 2004, pp. 3295–3301.

[19] V. Ruiz Garate, M. Pozzi, D. Prattichizzo, N. Tsagarakis, and A. Ajoudani, "Grasp Stiffness Control in Robotic Hands Through Coordinated Optimization of Pose and Joint Stiffness," *IEEE Robotics and Automation Letters*, vol. PP, pp. 1–1, 2018.

[20] V. Ruiz Garate, M. Pozzi, D. Prattichizzo, and A. Ajoudani, "A bio-inspired grasp stiffness control for robotic hands," *Frontiers in Robotics and AI*, vol. 5, p. 89, 2018.

[21] A. Ajoudani, N. G. Tsagarakis, and A. Bicchi, "Choosing Poses for Force and Stiffness Control," *IEEE Transactions on Robotics*, vol. 33, no. 6, pp. 1483–1490, 2017.

[22] S. Chiu, "Task Compatibility of Manipulator Postures," *I. J. Robotic Res.*, vol. 7, pp. 13–21, 1988.

[23] W. Friedl and M. A. Roa, "CLASH—A Compliant Sensorized Hand for Handling Delicate Objects," *Frontiers in Robotics and AI*, vol. 6, p. 138, 2020.

[24] T. Wimböck, C. Ott, and G. Hirzinger, "Impedance Behaviors for Two-Handed Manipulation: Design and Experiments," in *IEEE Int. Conf. on Robotics and Automation*, 2007, pp. 4182–4189.